Estimation of profiles of the effective ion charge at ASDEX Upgrade with Integrated Data Analysis

S.K. Rathgeber, R. Fischer, S. Fietz, J. Hobirk, A. Kallenbach, H. Meister, T. Pütterich, F. Ryter, G. Tardini, E. Wolfrum, and the ASDEX Upgrade Team

MPI für Plasmaphysik, Boltzmannstr. 2, D-85748 Garching, EURATOM-Association, Germany

E-mail: sylvia.rathgeber@ipp.mpg.de

Abstract.

The knowledge of the effective ion charge Z_{eff} which indicates the degree of plasma pollution is of high interest, since the tolerable impurity concentration to achieve successful ignition of a fusion plasma is limited. The quantification of Z_{eff} at ASDEX Upgrade has been carried out by means of Integrated Data Analysis in the framework of Bayesian Probability Theory which allows the combined analysis of different bremsstrahlung and charge exchange diagnostics to obtain one joint Z_{eff} profile. With this tool it is possible to assess the quality of the data acquired by the individual diagnostics and to find a reasonable selection of data for the routine Z_{eff} analysis. The Z_{eff} results are validated by the examination of different discharge scenarios and successfully applied to simulations of the neutron rate and the loop voltage. The investigation of Z_{eff} for nitrogen seeded discharges reveals a correlation between the confinement improvement and the increase of Z_{eff}.

1. Introduction

The effective ion charge Z_{eff} is the commonly used quantity to characterise the impurity content of a plasma. It is defined as the averaged charge,

$$Z_{\text{eff}} = \frac{\sum_i n_i Z_i^2}{\sum_i n_i Z_i} = \frac{\sum_i n_i Z_i^2}{n_e}, \tag{1}$$

of all present ions in the charge state Z_i, where n_e is the electron and n_i the ion density of species i. Z_{eff} has to be kept below a certain value – e.g. at ITER between 1.6 and 2.0 depending on the discharge scenario [1] – because an increasing impurity concentration leads to an enhancement of plasma dilution and of energy losses via bremsstrahlung and line radiation. [2]

These two types of radiation are measured via bremsstrahlung and charge exchange diagnostics and the dependency of their intensities on the ion charge are used to estimate Z_{eff}. Former work considered these different methods to estimate Z_{eff} separately [3] – at ASDEX Upgrade mostly in terms of a deconvolution algorithm for the line integrated bremsstrahlung intensity in the visible spectral range [4]. At the Joint European Torus (JET) tokamak, the

analysis of the visible bremsstrahlung only allows for inferences on averaged Z_{eff} values. Instead, Z_{eff} profiles are obtained via tomography of bremsstrahlung in the x-ray region or via charge exchange measurements of the impurities [5]. Each diagnostic has different advantages and disadvantages and they do not always lead to consistent results [6].

The current Z_{eff} analysis at ASDEX Upgrade facilitates to consider bremsstrahlung and line radiation data at the same time. Applying the concept of Integrated Data Analysis (IDA) – the joint treatment of several diagnostics – in the framework of Bayesian Probability Theory (BPT) enables to achieve more reliable results and a more consistent error analysis.

In section 2 the charge exchange and bremsstrahlung diagnostics used for this analysis are presented. Section 3 gives a review on Bayesian Probability Theory and its implementation to the calculation of Z_{eff}. Several Z_{eff} results for different combined data sets, displayed in section 4, demonstrate the benefits of IDA. It allows to assess the quality of different data, to reveal deficits of the individual diagnostics and, therefore, to create a reasonable selection of data for routine analysis. The quality of the results is validated in section 5 regarding two different types of discharge scenarios – standard H-mode and helium discharges. Finally, in section 6 the Z_{eff} analysis is applied to the simulation of the loop voltage and to nitrogen seeded discharges. The latter are currently of great interest due to their improved confinement which is still not fully understood.

2. Diagnostics

The diagnostics which are used for the evaluation of Z_{eff} are named CER, CHR, CMR and ZEB. The location of their lines of sight (LOS) in the torus of ASDEX Upgrade is shown in Figure 1. The CER and CHR [7] diagnostic, view the main plasma up to the magnetic axis (black, dashed) in the centre of the plasma. CMR [8] and ZEB [4] are edge diagnostics. Like the core diagnostics they are positioned at the low field side. A short description of the diagnostics is given in Table 1.

The dotted orange lines in sectors 7 and 15 (red numbers) represent the centres of the beams of neutral particles which are injected to heat the plasma. The gas valves for the deuterium fuelling of the plasma are located in sectors 1, 9 and 13.

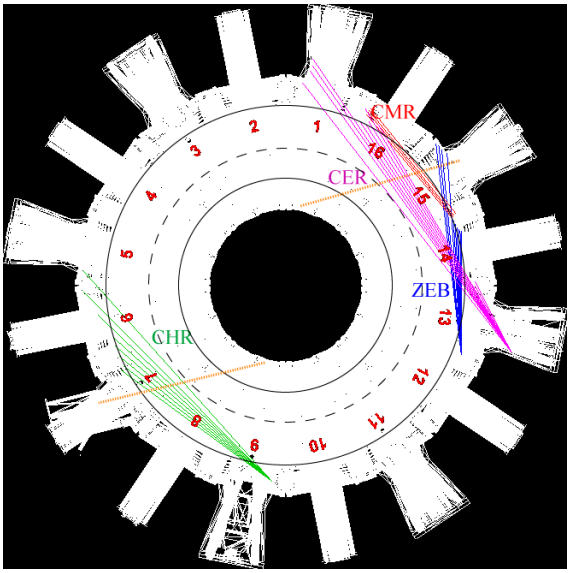

Figure 1. Location of diagnostics (coloured, solid), the neutral beams (orange, dotted), the plasma borders (black, solid) and the magnetic axis (black, dashed)

For each of the diagnostics the radiation emitted along the LOS is measured in dedicated

wavelength ranges using a Czerny-Turner spectrometer and a CCD camera. The intensity is absolutely calibrated using a calibrated integrating sphere which is placed inside the vessel in front of the optics and, therefore, considers all optic components. The calibration is carried out at the beginning and the end of each campaign. In case of considerable modifications in the calibration coefficient during the campaign (up to 15 % have been observed) the data are recalculated.

	CER	CHR	CMR	ZEB
Principle	Charge Exchange Recombination Spectroscopy			Bremsstrahlung measurement
LOS	11	9	8	9
Location	plasma centre		plasma edge	
Mostly observed wavelength ranges	$526-532\,nm\,(C^{5+}, n=7\rightarrow 8)$ $564-570\,nm\,(N^{6+}, n=8\rightarrow 9)$			$532-562\,nm$
Mostly used time resolution	$50\,ms$		$1.9\,ms$	$60\,ms$
Detector	Czerny-Turner spectrometer and CCD camera			

Table 1. Overview of diagnostics

2.1. Charge Exchange Recombination Spectroscopy

CER, CHR and CMR are Charge eXchange Recombination Spectroscopy (CXRS) diagnostics which serve as a measurement of single spectral lines belonging to different impurity species. After receiving an electron by charge exchange with neutral particles (mostly deuterium) from the Neutral Beam Injection (NBI) heating system the impurity ions emit characteristic line radiation. The radiation intensity of this specific transition allows to deduce the density of the corresponding ion species [9]. With known concentrations of all impurities Z_{eff} can be calculated according to Equation 1.

One difficulty to estimate Z_{eff} via the line radiation is that the accurate assignment of the line intensities might be complicated due to overlapping spectral lines of different species or further contributions from bremsstrahlung or recombination radiation. However, the main drawback of this method is the requirement of a separate diagnostic for each single impurity to receive the densities of all species simultaneously. Even if only the main impurities were considered this would demand a substantial experimental effort.

2.2. Bremsstrahlung

The necessity to know the concentration of each impurity species is omitted in the Z_{eff} analysis via the bremsstrahlung. The relation between the line integrated bremsstrahlung and Z_{eff} is

given by:

$$B_{\mathrm{LOS}} = \int_{\mathrm{LOS}} dl \int_0^\infty d\lambda\, C\, \overline{g}(\lambda, T_e, Z_{\mathrm{eff}})\, \frac{n_e^2 Z_{\mathrm{eff}}}{\sqrt{k_{\mathrm{B}} T_e}}\, \frac{\exp\left(-\frac{hc}{\lambda k_{\mathrm{B}} T_e}\right)}{\lambda^2}. \tag{2}$$

Therefore, measuring the bremsstrahlung intensity B_{LOS} along the LOS while knowing the electron density n_e, temperature T_e and the averaged gaunt factor $\overline{g}$ provides the possibility to estimate Z_{eff}. The averaged gaunt factors are calculated according to [10] and, for efficient calculations, supplied in a tabulated form depending on the wavelength, the electron temperature and Z_{eff}. [2]

The charge exchange spectra do not only provide information about the line radiation itself – additionally, the assessment of their background radiation can be used as a measure of the bremsstrahlung intensity. The problem is to differentiate this background from active or passive spectral lines. Assuming that there are spectral intervals with signals only caused by bremsstrahlung its emission intensity can be estimated in different ways. One possibility is to assess the bremsstrahlung signal only from these intervals while the other wavelength ranges are discarded. The alternative is to employ an outlier robust technique which can be applied to the full spectrum without censoring of the data. This is especially useful if large amounts of data have to be analysed routinely.

Both methods rely on the $1/\lambda^2$ dependency of the bremsstrahlung emission and on the knowledge about the measurement errors. The difference consists in the used likelihood probability distributions. The first method usually applies a Gaussian likelihood valid for independent and normally distributed uncertainties. This likelihood can no longer be used if systematic errors or additional signal contributions, e.g. line radiation, occurs. The second approach is based on mixture modelling with a likelihood consisting of two parts: A Gaussian and a marginalized Gaussian likelihood which allows for additional but unspecified signals. An elaborate analysis of the statistical measurement uncertainties allows to separate statistical noise from line emission. With this outlier robust method the bremsstrahlung emission can be estimated in the presence of line intensity and a probability can be calculated if the measured intensity at a given wavelength is only due to bremsstrahlung or polluted with additional signals. No data censoring prior to the analysis is necessary. The contaminated signals are mitigated automatically. Details about the method can be found in [11].

Two examples of such fits to carbon spectra are shown in Figure 2. As already mentioned the applicability of those fit methods requires regions of radiation which purely consist of bremsstrahlung. With spectral resolutions better than $R = \frac{\nu}{\Delta\nu} = 5000$ the CXRS diagnostics are capable to resolve even the single lines of molecular bands and, therefore, to fulfil the constraint of pure bremsstrahlung regions. This can be seen in the right hand spectrum whose background can be fitted quite well. Anyway, under certain circumstances, which will be discussed in subsection 4.1, the whole measured frequency range is polluted by overlapping small lines as for discharge #23757. This leads to an overestimated bremsstrahlung background.

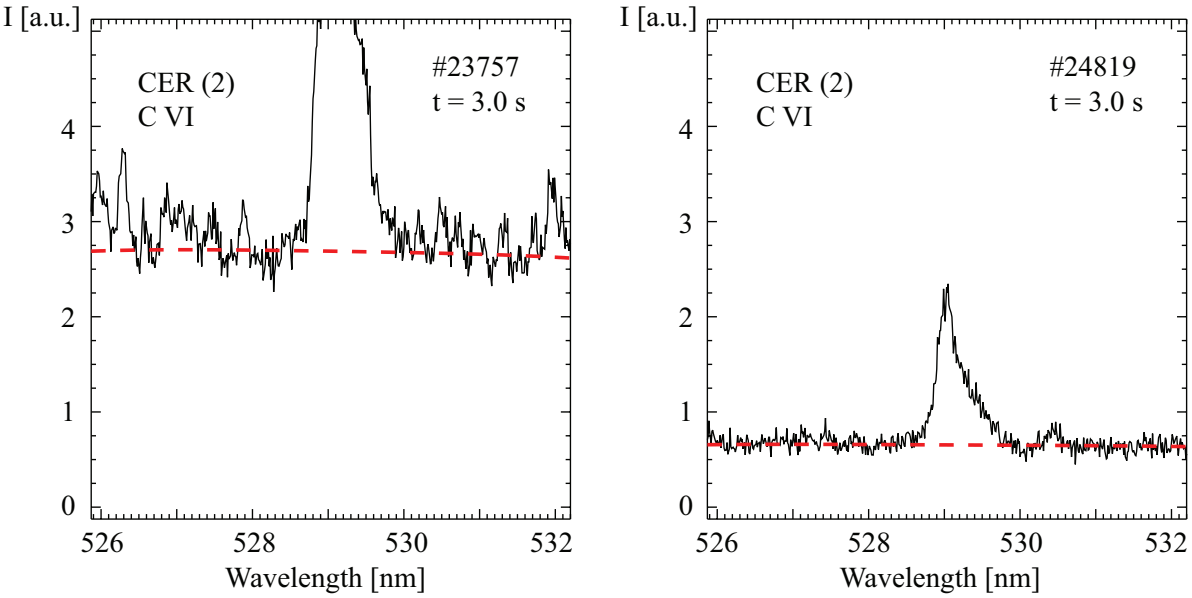

Figure 2. Bremsstrahlung fits (red, dashed) to the C VI spectra (black, solid) of discharge #23757 and #24819 each for LOS 2 of the CER

The ZEB diagnostic does not intersect with the neutral beam. Hence, it measures only the line integrated background radiation, usually in the wavelength range between 532 and 562 *nm*. This is above the region of recombination radiation and below the region where thermal radiation of hot vessel components in the infrared spectral range becomes relevant. Additionally, this range is not strongly affected by line radiation. The same fit algorithm as for the CXRS spectra is applied to exclude non-bremsstrahlung contributions, like weak tungsten lines, lines of molecular bands, etc. It is assumed that for the observed frequency range the latter ones are restricted to the Fulcher bands of D_2 [12]. Their line densities might exceed the resolution capability ($R = 3000$) of the ZEB but since they do not cover the whole region of interest the fit method is still applicable.

3. Estimation of Z_{eff}

The assessment of Z_{eff} within the concept of IDA employs BPT. Augmenting the statistical interpretations of frequency distributions, probability in terms of Bayes serves as a measure of the validity of a random or non-random quantity. This allows to include presumptions (a priori information) about the quantity of interest which are independent of the experimental measurements. Quantified by the *prior function* $p(\theta)$ this previous knowledge about the quantity of interest – parameterised by θ – is linked with the experimental data y – considered within the *likelihood function* $p(y|\theta)$ – via Bayes Theorem $p(\theta|y) = \frac{p(y|\theta)p(\theta)}{p(y)}$. The conditional probability $p(\theta|y)$ of the parameter values θ for a given data set y is called *posterior function*. The position of its maximum indicates the parameter values that are most likely to produce the measured data. Since in this case the evidence $p(y)$ is just a normalisation and, therefore, does not influence the location of the maximal posterior value, it does not have

to be considered. [13]

Applying Bayes Theorem to the estimation of Z_{eff} results in:

$$p(Z_{\mathrm{eff}}|d) \propto p(d|Z_{\mathrm{eff}})p(Z_{\mathrm{eff}}) \tag{3}$$

with the jointly measured data d of the bremsstrahlung and the CXRS diagnostics. Since IDA enables the linkage of several diagnostics for a combined analysis, the posterior distribution arises from the product of the individual likelihood functions of the different diagnostics and the joint prior function:

$$Posterior \propto L_{\mathrm{CER}} \times L_{\mathrm{CHR}} \times L_{\mathrm{CMR}} \times L_{\mathrm{ZEB}} \times L_{\mathrm{CXR}} \times Prior. \tag{4}$$

For the likelihood functions L_{CER}, L_{CHR}, L_{CMR} and L_{ZEB} containing the bremsstrahlung data Gaussian distributions are chosen. They compare the measured line integrated bremsstrahlung intensity b_{LOS} with the modelled bremsstrahlung intensity B_{LOS} and weight the deviation with the error of the measurement Δb_{LOS}: $L = p(b_{LOS}|Z_{\mathrm{eff}}) \propto \prod_{\mathrm{LOS}} \exp\left\{-\frac{1}{2}\left(\frac{B_{\mathrm{LOS}}-b_{\mathrm{LOS}}}{\Delta b_{\mathrm{LOS}}}\right)^2\right\}$. The modelled bremsstrahlung intensity is given by Equation 2. The electron temperature and density profiles are estimated separately within the concept of IDA [14, 15, 16], using the data of the lithium beam impact excitation spectroscopy, the DCN interferometry and the Electron Cyclotron Emission diagnostic.

Z_{eff} is parameterised with $Z_{\mathrm{eff}} = 1 + \exp(spline)$, where a cubic B-spline over seven parameter values at equidistant ρ_{pol} values between 0 and 1.2 is used. $\rho_{\mathrm{pol}} = \sqrt{\frac{\Psi-\Psi_{axis}}{\Psi_{separatrix}-\Psi_{axis}}}$ is the minor radius normalised on the poloidal magnetic flux Ψ. This parametrisation of Z_{eff} already includes the prior information that Z_{eff} cannot be smaller than 1. Additional to this hard constraint another soft condition is explicitly given by the prior function: Z_{eff} values higher than an upper boundary $Z_{\mathrm{eff,up}}$ – which are assumed to be unlikely at most time points of a discharge – are penalised by the prior function $p(Z_{\mathrm{eff}}) \propto \prod_j \exp\left\{-\frac{1}{2}\left(\frac{Z_{\mathrm{eff},j}-Z_{\mathrm{eff,up}}}{\Delta Z_{\mathrm{eff,up}}}\right)^2\right\}$ for $\rho_{\mathrm{pol},j}$ with $Z_{\mathrm{eff},j} > Z_{\mathrm{eff,up}}$ and $p(Z_{\mathrm{eff}}) = 1$ elsewhere. Typical values of $Z_{\mathrm{eff,up}} = 10$ and $\Delta Z_{\mathrm{eff,up}} = 1$ are chosen for routine analysis and for all the results shown in this paper. For specific applications like the examination of the loop voltage at the very beginning of a discharge (cf. section 6), these values can be relaxed or even omitted. A beneficial side effect of this Prior is the increased numerical robustness of the optimisation scheme to find the posterior maximum.

The data of the line radiation is considered within the likelihood L_{CXR}. It compares the parameter values of Z_{eff} with the values z_{eff} given by the sum of all impurity densities according to Equation 1: $L_{\mathrm{CXR}} = p(z_{\mathrm{eff}}|Z_{\mathrm{eff}}) \propto \prod_j \exp\left\{-\frac{1}{2}\left(\frac{Z_{\mathrm{eff},j}-z_{\mathrm{eff},j}}{\Delta z_{\mathrm{eff},j}}\right)^2\right\}$. The uncertainties Δz_{eff} are given by Gaussian error propagation of the uncertainties of the individual impurity densities.

An estimate for Z_{eff} is given by the value which maximises the posterior. This maximum can be determined by finding modelled values D that are consistent with the experimental data d within the error of the measurement and that satisfy the prior condition at the same time. A possibility to check the consistency of the modelled data is given by the residuals $res = \frac{D-d}{\Delta d}$.

Residual values between +1 and -1 imply that the modelled data fit the measured ones within their uncertainties.

For the error estimation of the parameter values, the posterior function is approximated with a normal distribution. The curvature at its maximum, given by the Hessian matrix, then specifies the $1\,\sigma$ uncertainties. To quantify the error of Z_{eff}, Gaussian error propagation is applied to include the uncertainties of the electron density and – in case of considering the bremsstrahlung data – the electron temperature as well. Since the bremsstrahlung depends quadratically on the electron density while the temperature shows a square root dependency, the uncertainties in the density are most important. With typical uncertainties of 10 % the electron density delivers the main contribution to the error bars of Z_{eff}.

4. Data validation

The following Z_{eff} profiles serve as a demonstration of the possibility to get consistent results with the combined analysis of different diagnostics and of the capability of IDA to assess the quality of the data and to reveal deficits of the individual diagnostics. As the aim of this chapter is the evaluation of the measured data and the statistical method, this discussion does not include details of the discharge characteristics. Both discharges treated in subsection 4.1 will be examined again in section 5.

4.1. Combined bremsstrahlung data

Figure 3(a) shows the Z_{eff} profile of discharge #23619 which allows a consistent combined analysis of three diagnostics – CER, CHR and ZEB. In Figure 3(b) the respective bremsstrahlung data of the different diagnostics are plotted. The measured line integrated bremsstrahlung intensity is represented by a solid black line, together with the modelled one dashed in red against the line of sight, respectively its minimal ρ_{pol} value. Additionally, the residuals are plotted with green dots. With values mostly between +1 and -1, the residuals imply that the data of all three diagnostics are consistent.

However, not all LOS are considered for the estimation of this Z_{eff} profile. Due to different reasons the data of some channels or a whole diagnostic cannot be used for the analysis. For instance, strong deuterium influx by gas valves, fuelling the plasma, perturbs the bremsstrahlung signal and, hence, LOS passing close to an employed gas valve yield unreliable results. The influence of the fuelling on the background radiation is demonstrated in Figure 2. Both spectra are measured with the second innermost channel of the CER. Due to the usage of the valve in sector 13 (cf. Figure 1) – which is assumed to result in an enhanced local density of neutrals – for discharge #23757, its spectrum shows much more passive lines, belonging to transitions of neutrals after (electron) impact excitation, than the one of discharge #24819, which was fuelled by other valves. These overlapping signals are difficult to separate from the bremsstrahlung background which is, therefore, overestimated. Since most discharges utilise the valves in sectors 1 and 13 near the CER and ZEB diagnostic, their data are not routinely applied for the Z_{eff} analysis. The helium discharge #23619 was

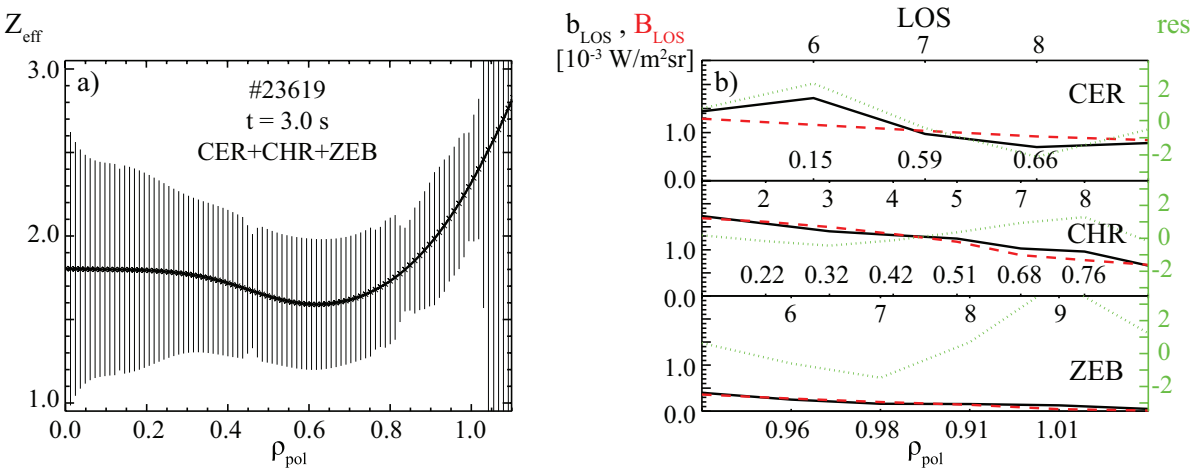

Figure 3. (a) Z_{eff} profile and (b) respective measured (black, solid) and modelled (red, dashed) bremsstrahlung intensity and residuals (green, dotted) of CER, CHR and ZEB data for discharge #23619

fuelled by the valve in sector 9.

Another problem is the occurrence of systematically overestimated bremsstrahlung values for some LOS which might be the result of reflections at vessel components (cf. [2, 6, 17]).

This is mainly observed for channel six of CHR, which views a curved vessel surface (cf. Figure 4). Also channels seven and eight – which intersect with a plane surface, while the other ones view non plasma-facing components or complex structures – tend to be slightly overestimated for some discharges. However, since channel six is affected by reflections mostly and routinely it is the only one not considered for the estimation of Z_{eff}.

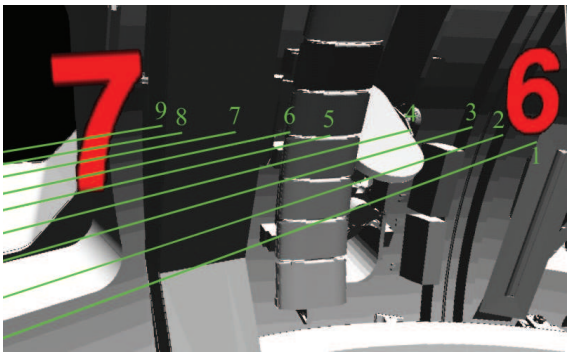

Figure 4. Positions of LOS of CHR

The CMR diagnostic is an ideal candidate for providing edge bremsstrahlung information with high temporal resolution of 1.9 ms. However, due to these short exposure times and the low density at the plasma edge, the bremsstrahlung intensity is very small and noisy which makes its separation from passive lines and continuum radiation challenging. Resulting systematic errors are particularly harmful due to the large number of data as illustrated in Figure 5(b). The CMR bremsstrahlung values of discharge #23406 seems to be systematically underestimated. Although these low edge values are not consistent with the CHR data they dominate the estimation of the edge Z_{eff} values (cf. solid line in Figure 5(a)). Nevertheless, within the error bars the Z_{eff} profile obtained via the combined data of CHR and CMR is consistent with the one including only the CHR data (cf. Figure 8(a)).

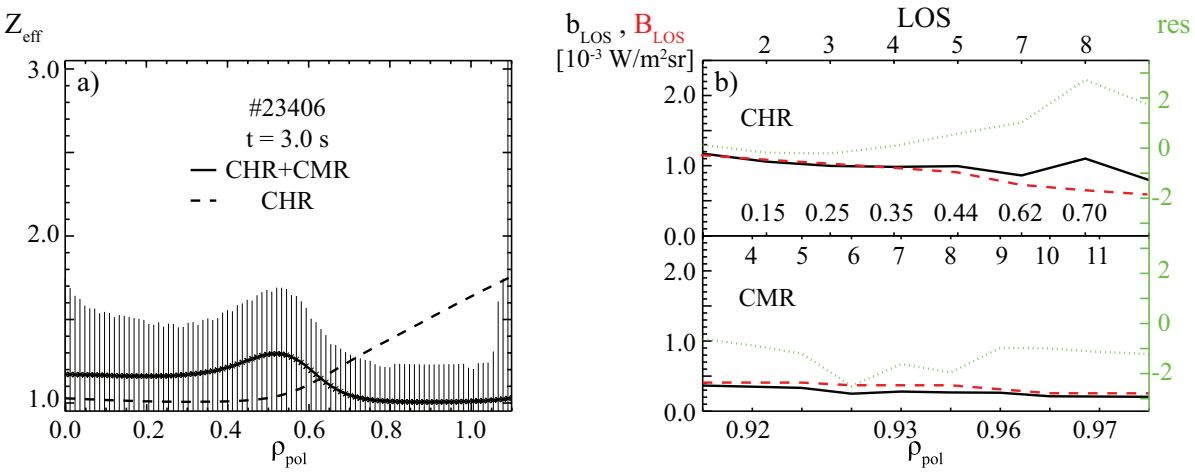

Figure 5. (a) Z_{eff} profile of CHR data alone (dashed) and of combined CHR and CMR data (solid) and (b) measured (black, solid) and modelled (red, dashed) bremsstrahlung intensity and residuals (green, dotted) of combined CHR and CMR data for discharge #23406

According to this discussion the CHR diagnostic is – apart from its sixth channel – the most reliable one for the Z_{eff} analysis and, therefore, the only one used for routine analysis.

4.2. Bremsstrahlung vs. line radiation

The Z_{eff} profiles determined from the bremsstrahlung data are now compared with the profiles from CXRS line emission data. These two methods are known that they might produce inconsistent results [6].

The estimated impurity densities for discharge #23782 result in the dashed Z_{eff} profile in Figure 6(a). The dominating impurities – nitrogen and carbon – are measured via the CXRS diagnostic. Their contributions to Z_{eff} are plotted in Figure 6(b) (nitrogen: blue diamonds, carbon: orange triangles), as well as the absolute Z_{eff} values (black, solid) given by the deuterium background and the sum of all impurities which additionally includes approximations for oxygen (0.05 %), fluorine (0.05 %) and boron (0.5 %). The calculated Z_{eff} profile is represented by the red dashed curve. Within the error bars, it is consistent with the result from the bremsstrahlung, the solid line in Figure 6(a), but it shows a different shape. While the bremsstrahlung data regularly lead to a hollow Z_{eff} profile, the measured impurity concentrations for this discharge result in a peaked profile.

Other discharges show rather flat or slightly hollow Z_{eff} profiles according to the line radiation. For instance, in discharge #25391 the nitrogen concentration – the dominating and only measured impurity – results in a slightly hollow profile shown as a dashed line in Figure 7(a). However, there is a remaining discrepancy to the Z_{eff} profile obtained by the bremsstrahlung data of CHR (solid line) at the plasma edge. Here, it should be remarked that according to transport modelling at the plasma edge the assumption of fully ionised impurities with $Z < 10$ is a good approximation within $\rho_{\mathrm{pol}} = 0.95$ where electron temperatures are higher than $500\,eV$. Impurities with $Z > 10$ are observed at low enough concentrations such that a contribution to Z_{eff} can be ignored.

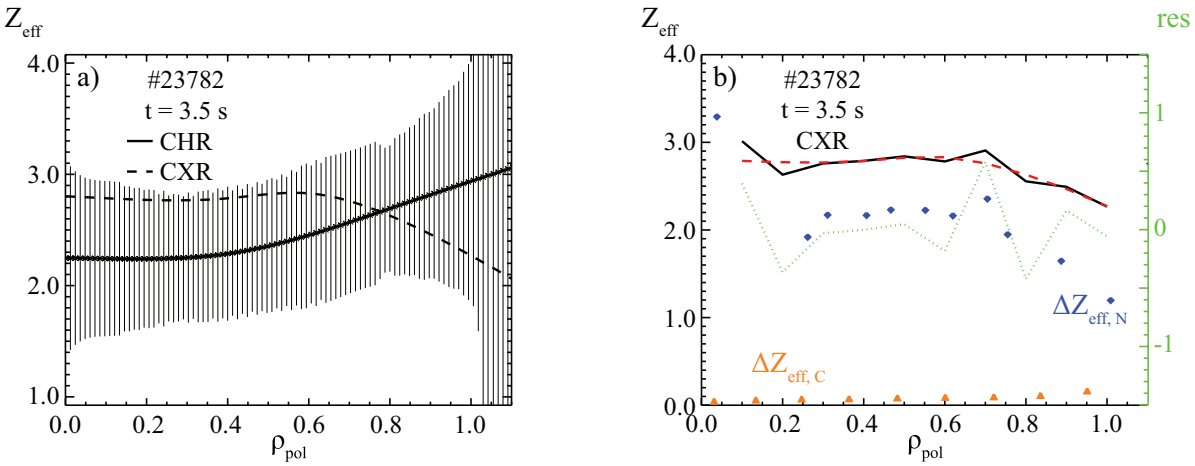

Figure 6. (a) Z_{eff} profiles via bremsstrahlung data of CHR (solid) and via impurity concentration (dashed) and (b) respective measured (black, solid) and spline fitted (red, dashed) Z_{eff} values, the contribution of nitrogen (blue diamonds) and carbon (orange triangles) to Z_{eff} and the residuals (green, dotted) for discharge #23782

To assess the validity of the results obtained with bremsstrahlung and line radiation against each other, the profiles of discharge #23782 are utilised for the simulation of the neutron rate. The simulation results are then compared with the measured neutron rate. At ASDEX Upgrade the neutron rate is dominated by beam-target reactions and can be estimated according to $S_{\mathrm{bt}} \propto T_e^{3/2} \frac{n_{\mathrm{D}}}{n_e} P_{\mathrm{NBI}}$ [18]. The rate is proportional to the deuterium density divided by the electron density and, therefore, dependent on Z_{eff}. The results of the simulations with the transport code TRANSP [19] are presented in Figure 7(b). The dashed red line describes the time trace of the simulated total neutron rate that includes the bremsstrahlung Z_{eff}, the dashed blue line the one with Z_{eff} via the line radiation.

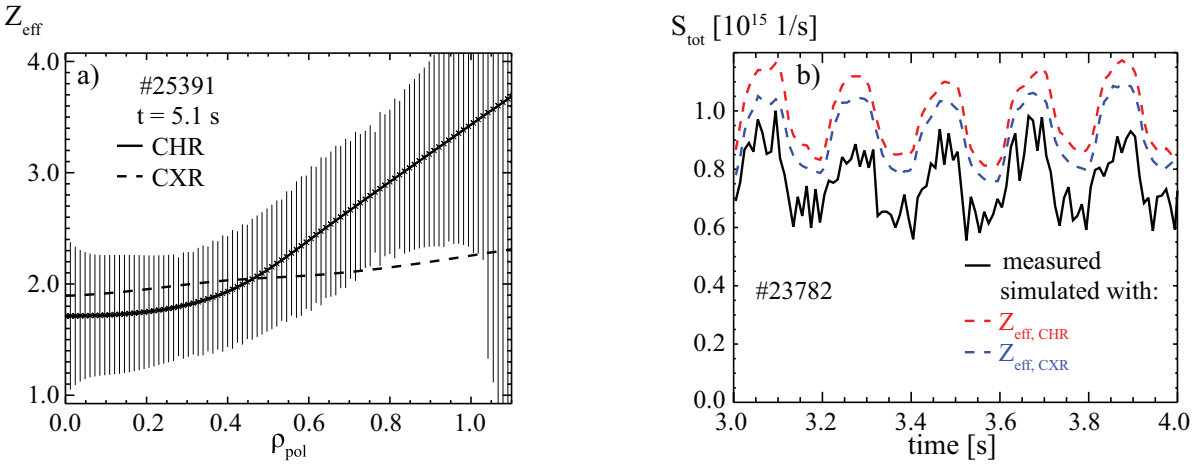

Figure 7. (a) Z_{eff} profiles of discharge #25391 via bremsstrahlung data of CHR (solid) and via nitrogen concentration (dashed) and (b) time traces of measured (black, solid) and simulated (red, dashed: with Z_{eff} via bremsstrahlung; blue, dashed: with Z_{eff} via line radiation) total neutron rate for discharge #23782

The oscillation of the simulated neutron rate, as well as the measured one (black, solid) is the result of the NBI modulation which uses two alternating beams with different beam energies. The fact that the simulated neutron rate is about 20 % higher than the measured one is generally observed and is assumed to be a systematic effect of overestimated fast particles which, according to the simulation, account for around 5 % of the electron density in the core plasma down to 0 at the edge. Given that the difference between both simulations is smaller than their deviation from the measurement, it is not possible to predict which one of the profiles provides the better simulation input.

Therefore, it remains unresolved whether the bremsstrahlung or the line radiation delivers the more reliable Z_{eff} results. Anyway, since the diagnostic capabilities to estimate all impurity concentrations simultaneously are restricted, only the bremsstrahlung data is used for the routine estimation of Z_{eff}.

5. Validation of results

The quality of the Z_{eff} results, obtained via IDA and according to the previously justified data selection, is validated for two different types of discharges. The estimated Z_{eff} values for standard H-mode and helium discharges both are consistent with the expected values.

5.1. Standard H-mode discharges

Figure 8(a) shows the Z_{eff} profile of discharge #23406. This standard H-mode discharge with plasma current $I_P = 1.0\,MA$, toroidal magnetic field $B_t = -2.5\,T$ and a central electron density of $n_{e,0} = 9.4 \times 10^{19}\,m^{-3}$ was carried out shortly after a boronisation and, therefore, a low impurity content is expected. This is confirmed by the estimated Z_{eff} values below 1.6 within the separatrix. Up to $\rho_{\mathrm{pol}} = 0.5$ Z_{eff} is actually close to 1.0 as for a pure deuterium plasma.

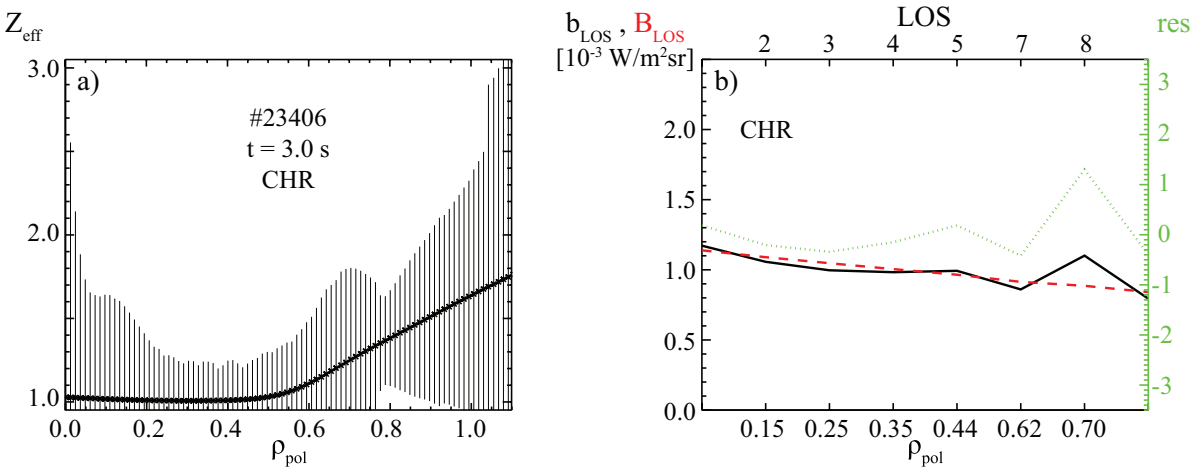

Figure 8. (a) Z_{eff} profile and (b) respective measured (black, solid) and modelled (red, dashed) bremsstrahlung intensity and residuals (green, dotted) of CHR for discharge #23406

It is interesting to note that not even in this region the residuals of the bremsstrahlung

shown in Figure 8(b) do reach values below -1 which means that the deviation of the modelled data to smaller values than the measured ones is within the error bars. This indicates that the Z_{eff} values close to 1 are not an effect of the constraint that Z_{eff} must not be smaller than 1, but actually consistent with the data.

5.2. Helium discharges

Another possibility to validate the Z_{eff} results is provided by helium discharges. Knowing the helium concentration and assuming that there are no other impurities, Z_{eff} can be calculated according to Equation 1. At ASDEX Upgrade the helium concentration is measured with the Visible Survey Spectrometer (VSS) in the divertor. Due to the higher compression of hydrogen in the divertor compared to the one of helium, the helium concentration in the divertor differs from the one in the main chamber. As an estimate for the helium concentration in the main plasma an upper and lower limit are found in agreement with the CXRS measurements. [20]

The comparison of Z_{eff} determined from the bremsstrahlung with the one calculated from the helium concentration was performed for discharge #23619. This discharge with plasma parameters $I_P = 1.0\,MA$, $B_t = -2.3\,T$ and $n_{e,0} = 9.1 \times 10^{19}\,m^{-3}$ was carried out without NBI heating to avoid additional deuterium influx and, therefore, enable a high helium concentration. The VSS data deliver a helium concentration of $67\,\%$ in the divertor and, according to the mentioned correction for the enrichment, of $81-89\,\%$ in the main chamber. This corresponds to a Z_{eff} value of around 1.9 which is close to the result of the bremsstrahlung data in Figure 3(a) and is thus a good validation for the Z_{eff} analysis.

6. Applications to physics investigations

6.1. Loop voltage

According to $U_{\text{Loop}} \propto \frac{I_{\text{P}}}{\sigma(T_e, Z_{\text{eff}})}$ [21] with the Hirshman-Sigmar conductivity σ, the loop voltage depends on Z_{eff} and, therefore, its simulation needs Z_{eff} as input parameter.

The results of such simulations using the transport code ASTRA [22] for the startup phase of discharge #22886 are shown in Figure 9(b). At the beginning of a discharge, the plasma exists in the limiter phase and, therefore, contains many impurities from the limiter surface, leading to high Z_{eff} values (cf. Figure 9(a)). The dashed lines in (b) represent the time traces of the simulated loop voltage for different Z_{eff} profiles, two constant ones (violet and blue) and in red the one according to the bremsstrahlung data. The comparison with the measured loop voltage (black, solid) shows a good consistency with the dotted blue line at around $0.2\,s$ and with the dashed violet line at $0.3\,s$ and after $0.6\,s$, but all together the best consistency between measurement and simulation is given by using the experimental Z_{eff} values. The agreement between the results of the experimental Z_{eff} and the constant one of 3.0 from $0.55\,s$ on can be explained with the averaged measured Z_{eff} values of $2.0-3.0$ at respective times.

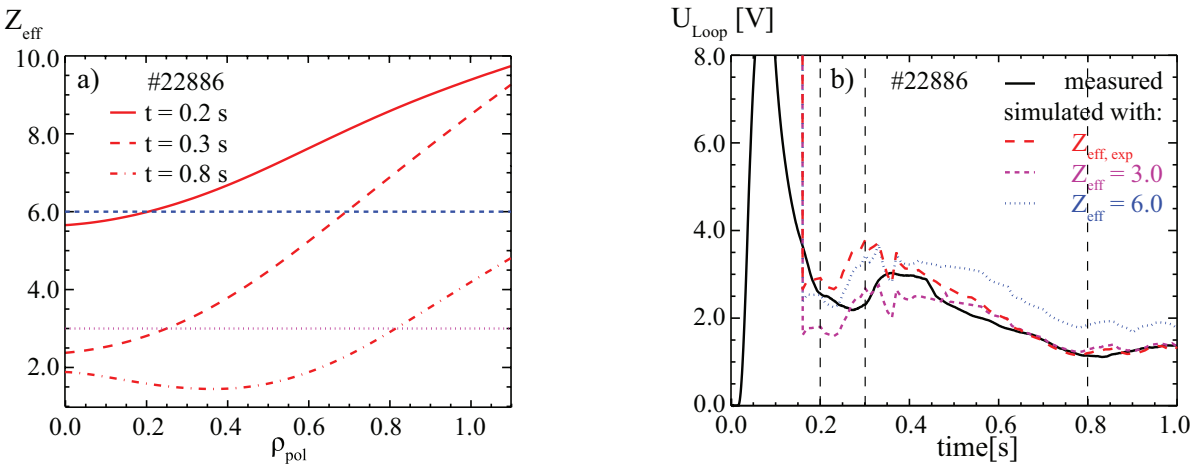

Figure 9. (a) Estimated Z_{eff} profiles (red) at three different time points and constant values used for the simulation and (b) time traces of measured (black, solid) and simulated loop voltage (red, dashed: with Z_{eff} via bremsstrahlung; violet, small dashed: with $Z_{\mathrm{eff}} = 3.0$; blue dotted: with $Z_{\mathrm{eff}} = 6.0$) for discharge #22886

6.2. Nitrogen seeded discharges

The fully tungsten coated machine ASDEX Upgrade needs impurity seeding in the divertor to reduce the heat flux on the target plates [23]. Beside this cooling effect, the seeding with nitrogen results in an improved plasma confinement [24]. This behaviour can be correlated with an increase of Z_{eff}. Therefore, several pairs of discharges with and without nitrogen seeding were analysed.

The Z_{eff} profiles of one of these pairs with identical plasma parameters $I_P = 1.0\,MA$, $B_t = -2.5\,T$ and $n_{e,0} = 9.2 \times 10^{19}\,m^{-3}$ are displayed in Figure 10(a). The nitrogen seeded discharge #24682 is plotted as a solid blue line, the reference discharge #24681 dashed in red. The expected enhancement of Z_{eff} with nitrogen seeding is stronger at the edge than in the core.

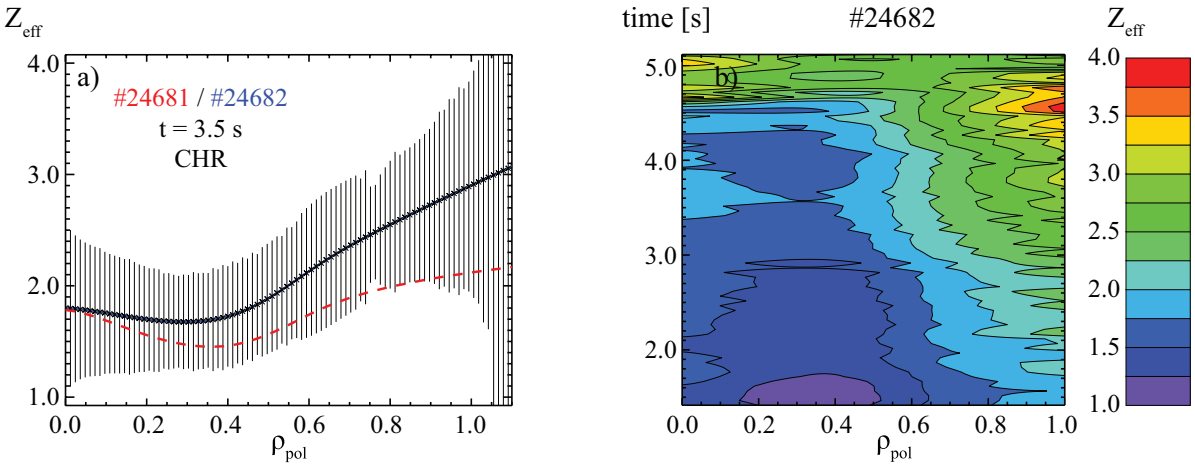

Figure 10. (a) Z_{eff} profiles of discharges #24681 (red, dashed) and #24682 (blue, solid) using CHR bremsstrahlung data and (b) contour plot of Z_{eff} for discharge #24682

Figure 10(b) shows the temporal evolution of the Z_{eff} profile with increasing nitrogen content. There is a considerable increase of Z_{eff}, starting at the edge and moving inwards, with the beginning of the nitrogen seeding at $1.7\,s$ and with its strong growth at $2.8\,s$. The corresponding time trace of the nitrogen influx Φ_{N} is displayed in Figure 11(b). Furthermore, with the abrupt enhancement of the core Z_{eff} at $4.7\,s$ Figure 10(b) nicely reveals the tungsten accumulation.

To compare the increase of Z_{eff} with the confinement enhancement, Figure 11 presents the time traces of Z_{eff} (d) at two different ρ_{pol} values (solid: 0.9, dashed: 0.2) together with the time trace of the H-factor (c), which is an indicator for the confinement. Additionally, the NBI heating power (a), the nitrogen and the deuterium influx (b) are plotted. The numbers mark the time intervals with constant plasma settings that are used in the following analysis.

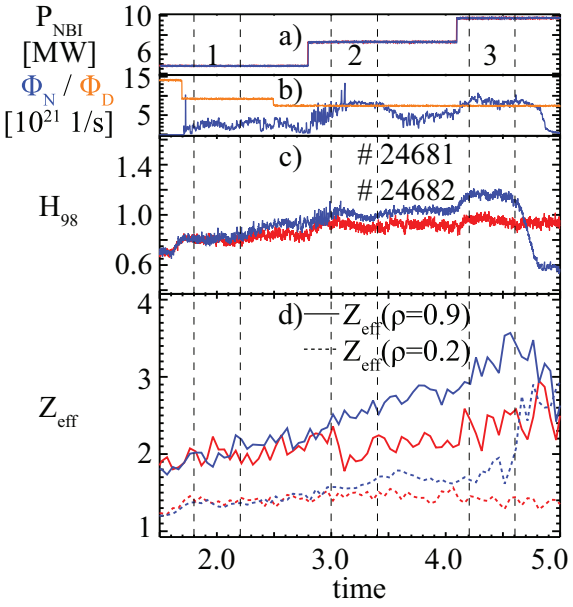

Figure 11. Time traces of (a) NBI heating power P_{NBI}, (b) deuterium Φ_{D} (orange) influx and nitrogen seeding Φ_{N} (blue), (c) H-factor H_{98} and (d) Z_{eff} at $\rho_{\mathrm{pol}} = 0.9$ (solid) and $\rho_{\mathrm{pol}} = 0.2$ (dashed) for nitrogen seeded discharge #24682 (blue) and its reference #24681 (red)

The H-factor increases for both discharges with rising heating power. Since the enhancement is much stronger in discharge #24682, even though the plasma settings are identical, the nitrogen seeding seems to have an influence on the confinement.

The correlation between Z_{eff} and H_{98} is illustrated in Figure 12. The H-factor of several nitrogen seeded discharges and one of their references is plotted against Z_{eff} at $\rho_{\mathrm{pol}} = 0.2/0.9$ (empty/full symbols). The plasma settings were identical during the examined time periods (described by different symbols) and only vary in the NBI heating power and the deuterium influx from one time period to another.

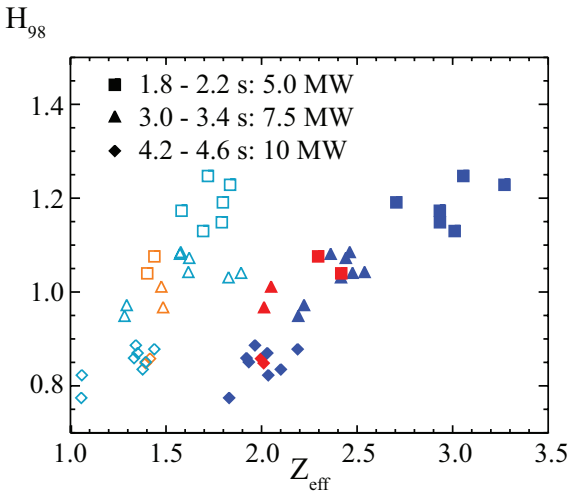

Figure 12. H-factor H_{98} for discharges with/without (blue/red) nitrogen seeding versus Z_{eff} at $\rho_{\mathrm{pol}} = 0.2/0.9$ (open/full symbols)

There is a considerable confinement improvement with increasing Z_{eff}. Regarding the

core Z_{eff} values, the relation is linear. For the edge Z_{eff}, the H-factor seems to saturate with a certain Z_{eff} value.

The H-factor is not a spatially resolved quantity. Thus, it is not possible to assign it to a local Z_{eff} value. Nevertheless, it is assumed that one contribution to the confinement improvement is a result of increased Z_{eff} at the edge, regarding the peeling-ballooning-limit [25]. According to this limit one expects equal edge pressure gradients for the nitrogen seeded discharges and their references. Additionally, the pedestal width is supposed to be the same, since the only dependencies found, the heating power [26] and the pedestal beta poloidal [27], are identical in both cases. As a result of these two assumptions of same pressure gradients and pedestal widths, also the total pressure values at the pedestal top should be equal for identical discharge conditions. This would allow to link the edge temperature enhancement of the seeded discharge with its deuterium dilution due to the nitrogen influx and, therefore, with the edge Z_{eff}. The observed stiff temperature profiles [28] and less dilution in the core, which is fulfilled for hollow Z_{eff} profiles, would cause a higher total pressure and, therefore, explain the confinement improvement. Detailed analysis to affirm this correlation is in progress.

7. Conclusion

As demonstrated, Integrated Data Analysis in the framework of Bayes Probability Theory provides the possibility to combine several diagnostics for one joint Z_{eff} profile. This enables to reveal deficiencies of the different diagnostics and, therefore, to find a reasonable selection of data. The selected data deliver consistent results and permit the routine generation of Z_{eff} profiles. Due to the identified limitations of some diagnostics for the Z_{eff} analysis, it is not possible to exploit the full potential of IDA. To avoid these restrictions of the measured data some modifications of the experimental setup might be useful. For instance, the relocation of the gas valves into the divertor which has been done for the next experimental campaign shall prevent the perturbation of the bremsstrahlung signals by the deuterium influx.

With the analysis of standard H-mode and helium discharges the range of the Z_{eff} values could be validated. Furthermore, it was pointed out that the simulations of the loop voltage and the neutron rate with Z_{eff} are consistent with the measurements. An interesting physics aspect was the correlation of the confinement improvement with enhanced Z_{eff} values. To validate the assumption that the confinement improvement arises from increased Z_{eff} values at the edge with respect to the peeling-ballooning-instability, further investigations of Z_{eff} in nitrogen seeded discharges are necessary.

[1] G. Verdoolaege, M.G. von Hellermann, R. Jaspers, M.M. Ichir, and G. Van Oost. Integrated Bayesian Estimation of Zeff in TEXTOR Tokamak from Bremsstrahlung and CX Impurity Density Measurements. In *Bayesian Inference and Maximum Entropy Methods in Science and Engineering*, volume 872, pages 541–548, 2006.

[2] H. Meister, R. Dux, L.D. Horton, B.Kurzan, P.J. McCarthy, H. Zohm, and ASDEX Upgrade Team. An integrated system to measure the effective charge of fusion plasmas in ASDEX Upgrade tokamak. *Review of Scientific Instruments*, 74:4625–4633, 2003.

[3] H. Meister, C. Angioni, B. Kurzan, C.F. Maggi, T. Pütterich, J. Schirmer, and ASDEX Upgrade Team.

Effect of density peaking on Zeff profiles in ASDEX Upgrade H-mode discharges. In *33rd EPS Conference on Plasma Physics. Contributed Papers*, volume 30 I, pages P–2.138, 2006.

[4] H. Meister, R. Fischer, L.D. Horton, C.F. Maggi, D. Nishijima, ASDEX Upgrade Team, C. Giroud, K.-D. Zastrow, and JET-EFDA Contributors. Zeff from spectroscopic bremsstrahlung measurements at ASDEX Upgrade and JET. *Review of Scientific Instruments*, 75:4097–4099, 2004.

[5] H. Weisen, D. Pasini, A. Weller, and A.W. Edwards. Measurements of light impurity densities and Zeff in JET using x-ray tomography. *Review of Scientific Instruments*, 62:1531–1538, 1991.

[6] G. Verdoolaege, R. Fischer, G. Van Oost, and JET EFDA contributors. Potential of a Bayesian integrated determination of the ion effective charge via bremsstrahlung and Charge Exchange Spectroscopy in tokamak plasmas. to be published in IEEE Transactions on Plasma Science, 2010.

[7] C.F. Maggi, L.D. Horton, B. Zaniol, P. Franzen, H. Meister, D. Nishijima, A. Stäbler, and ASDEX Upgrade Team. Neutral beam energy scan experiments in ASDEX Upgrade for impurity ion density evaluation with CXRS. In *30th EPS Conference on Controlled Fusion and Plasma Physics. Contributed Papers*, volume 27 A, pages P–1.63, 2003.

[8] T. Pütterich, C.F. Maggi, L.D. Horton, R. Dux, B. Langer, E. Wolfrum, and ASDEX Upgrade Team. Fast CXRS-Measurements in the Edge Transport Barrier of ASDEX Upgrade. In *35th EPS Conference on Controlled Fusion and Plasma Physics. Contributed Papers*, volume 32 D, pages P–2.083, 2008.

[9] R.C. Isler. A Review of Charge-Exchange Spectroscopy and Applications to Fusion Plasmas. *Physica Scripta*, 35:650–661, 1987.

[10] W.J. Karzas and R. Latter. Electron Radiative Transition in a Coulomb Field. *Astrophysical Journal Supplement*, 6:167–212, 1961.

[11] R. Fischer, K.M. Hanson, V. Dose, and W. von der Linden. Background Estimation in Experimental Spectra. *Physical Review E*, 61:1152–1160, 2000.

[12] G.H. Dieke and R.W. Blue. The Fulcher Bands of HD and D2. *Physical Review*, 47:261–273, 1935.

[13] A. Gelman, J.B. Carlin, H.S. Stern, and D.B. Rubin. *Bayesian Data Analysis*. Chapman & Hall, 1980.

[14] R. Fischer, E. Wolfrum, J. Schweinzer, and ASDEX Upgrade Team. Probalistic lithium beam data analysis. *Plasma Physics and Controlled Fusion*, 50(8):085009 (26pp), 2008.

[15] R. Fischer, E. Wolfrum, C. Fuchs, and ASDEX Upgrade Team. Integrated density profile analysis in ASDEX Upgrade H-modes. In *35th EPS Conference on Plasma Physics. Contributed Papers*, volume 32 D, pages P–4.010, 2008.

[16] R. Fischer, A. Burckhart, N. Hicks, B. Kurzan, E. Wolfrum, and ASDEX Upgrade Team. Multiple diagnostic data analysis of density and temperature profiles in ASDEX Upgrade. In *36th EPS Conference on Plasma Physics. Contributed Papers*, volume 33 E, pages P–1.159, 2009.

[17] B. Schunke, G. Huysmans, and P. Thomas. Evidence of the influence of reflections on the Zeff profile measurements and their mitigation. In *31st EPS Conference on Plasma Physics. Contributed Papers*, volume 28 G, pages P–4.111, 2004.

[18] H. Zohm, H.-S. Bosch, O. Gruber, R. Neu, H.-P. Schweiss, A. Stäbler J. Stober, and ASDEX Upgrade Team. Neutron Production in High Performance Scenarios in ASDEX Upgrade. In *29th EPS Conference on Plasma Physics and Controlled Fusion. Contributed Papers*, volume 26 B, pages P–1.043, 2002.

[19] A. Pankin, D. McCune, R. Andre, G. Bateman, and A. Kritz. The tokamak Monte Carlo fast ion module NUBEAM in the National Transport Code Collaboration library. *Computer Physics Communications*, 159(3):157–184, 2004.

[20] H.-S. Bosch, D. Coster, G. Haas, A. Kallenbach, M. Kaufmann, K. Lackner, J. Neuhauser, S. de Pena Hempel, W. Poschenrieder, R. Schneider, ASDEX Upgrade Team, and ECRH-Teams NI, ICRH. Particle exhaust studies in ASDEX Upgrade. *Plasma Physics and Controlled Fusion*, 39:1771–1792, 1997.

[21] I.H. Hutchinson. *Principles of Plasma Diagnostics*. Cambridge University Press, 1987.

[22] J. Hobirk, R.C. Wolf, P.J. McCarthy, M. Foley, O. Gruber, H. Meister, W. Schneider, W. Ullrich, and ASDEX Upgrade Team. First Measurements of the Radial Electric Field with the Motional Stark Effect Diagnostic in ASDEX Upgrade. In *27th EPS Conference on Controlled Fusion and Plasma Physics. Contributed Papers*, volume 24 B, pages 984–987, 2000.

[23] A. Kallenbach, R. Dux, J.C. Fuchs, R. Fischer, B. Geiger, L. Giannone, A. Herrmann, T. Lunt, V. Mertens, R. Mc Dermott, R. Neu, T. Pütterich, S. Rathgeber, V. Rohde, K. Schmid, J. Schweinzer, W. Teutterer, and ASDEX Upgrade Team. Divertor power load feedback with nitrogen seeding in ASDEX Upgrade. *Plasma Physics and Controlled Fusion*, 52:055002(17pp), 2010.

[24] J.C. Fuchs, T. Eich, L. Giannone, A. Herrmann, A. Kallenbach, B. Reiter, and ASDEX Upgrade Team. Radiation Distribution During Impurity Seeding Experiments in the Full Tungsten ASDEX Upgrade. In *36th EPS Conference on Plasma Physics. Contributed Papers*, volume 33 E, pages P–1.147, 2009.

[25] J.W. Connor, R.J. Hastie, H.R. Wilson, and R.L. Miller. Magnetohydrodynamic stability of tokamak edge plasmas. *Physics of Plasmas*, 5:2687–2700, 1998.

[26] C.F. Maggi, R.J. Groebner, N.Oyama, R. Sartori, L.D. Horton, A.C.C. Sips, W. Suttrop, ASDEX Upgrade Team, A. Leonard, T.C. Luce, M.R. Wade, the DIII-D Team, Y. Kamada, H. Urano, JT-60U Team, Y. Andrews, C. Giroud, E. Joffrin, E. de la Luna, EFDA-JET Contributors for the Pedestal, Edge Physics, and the Steady State Operation Topical Groups of the ITPA. Characteristics of the H-mode pedestal in improved confinement scenarios in ASDEX Upgrade, DII-D, JET and JT-60U. *Nuclear Fusion*, 47:535–551, 2007.

[27] P.B. Snyder, N. Aiba, M. Beurskens, R.J. Groebner, L.D. Horton, A.E. Hubbard, J.W. Hughes, G.T.A. Huysmans, Y. Kamada, A. Kirk, C. Konz, A.W. Leonard, J. Lönnroth, C.F. Maggi, R. Maingi, T.H. Osborne, N Oyama, A. Pankin, S. Saarelma, G. Saibene, J.T. Terry, H. Urano, and H.R. Wilson. Pedestal stability comparison and ITER pedestal prediction. *Nuclear Fusion*, 49:085035(8pp), 2009.

[28] G. Tardini, R. Fischer, V. Igochine, A. Kallenbach, C.F. Maggi, R. Neu, T. Pütterich, S.K. Rathgeber, J. Schweinzer, and ASDEX Upgrade Team. Confinement enhancement in ASDEX Upgrade improved H-mode discharges with nitrogen seeding. In *36th EPS Conference on Plasma Physics. Contributed Papers*, volume 33 E, pages O–2.004, 2009.